Ultrasonic imaging of bubble motion in a fiber preform

Naim Samet, Pierre Marechal, Hugues Duflo

ACOUSTICS 2012

Ultrasonic imaging of bubble motion in a fiber preform

N. Samet, P. Marechal and H. Duflo

Laboratoire Ondes et Milieux Complexes,
samet_naim@yahoo.ca

During the Resin Transfer Molding (RTM) process, bubbles can appear and move between fibers and meshes. In this study, a monitoring method for the size and velocity of air bubbles using an ultrasonic phased array transducer is proposed. This method is tested in a flow of a known viscous silicone oil along a sample of fiber preform. By ultrasonic imaging the fiber preform immersed in a viscous flow, a position-time map (x_{fl}, t) is obtained for each acquisition date t_{acq}. These data could be converted to (x_{fl}, z, t_{acq}) data. The bubble motion is extracted from the raw data by separation of the static component from the dynamic part of the signal. As a result, a modified C-scan is obtained and both the instantaneous position and velocity of a bubble could be extracted in the (x, z) plane. Through these measures, the evolution of the bubbles is related to the processes that generate them in order to consider improvements to the RTM technique.

1 Introduction

Composite materials offer a good trade-off in terms of mechanical-performance-to-cost ratio [1]. Fiber reinforced polymer composite materials have promising application fields in industrial products, as well as in aeronautics. Nevertheless, these performances are closely linked to the raw constitutive materials and fabrication process. Previously several studies were managed on manufacturing conditions of composite materials and their properties [2-5]. Particularly, during the Resin Transfer Molding (RTM) process [6-7], more precisely the injection of the resin, air bubbles can appear and stay along fibers and/or between fiber fabrics [8]. Air bubbles can cause porosities and future mechanical defect [9]. Preliminary, the acoustical detection possibilities of air bubbles in a viscous fluid were validated [10]. In this work, we are interested in air bubbles between fibers and layers of fiber woven fabrics [11]. These fabrics are immersed in a viscous fluid model, mimicking the resin before polymerization. Thus, an experimental setup mimicking the fabrication process was elaborated, and its acoustical properties were characterized. Then, the pulse-echo response of an air bubble moving up between the glass fiber fabrics immersed in a viscous silicone oil is obtained using a high frequency phased array transducer. Eventually, a suitable signal processing of the raw data allows to extract both velocity and size of the moving air bubble.

2 Setup

The experimental setup (Figure 1) was built in order to observe fiber fabrics immersed in a fluid, with air bubbles sliding along and between fiber fabrics. For that, a 4 mm thick gap is fixed by a sealing joint between two blocks of 50mm thick of PMMA. The glass fiber fabrics immersed in a silicone oil are inserted in this gap and characterized using ultrasound. Pulse-echo signals are carried out using an Olympus Tomoscan pulse-echo phased-array processing system. A 128-element phased array transducer, operating at a 10MHz center frequency, was used to sweep various positions (focal laws), which were periodically refreshed (acquisition rate).

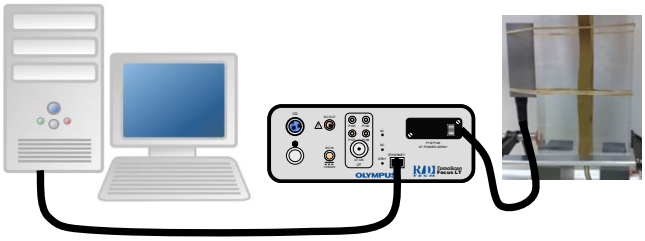

Figure 1: Experimental setup.

2.1 Setup characterization

In the acoustical point of view, transmission and reflection coefficients between media indexed p and q must be considered, $\underline{T}_{pq}$ and $\underline{R}_{pq}$ respectively.

$$\underline{T}_{pq} = \frac{2\underline{Z}_q}{\underline{Z}_q + \underline{Z}_p}, \quad (1)$$

and

$$\underline{R}_{pq} = \frac{\underline{Z}_q - \underline{Z}_p}{\underline{Z}_q + \underline{Z}_p}, \quad (2)$$

where $\underline{Z}_i = \rho_i.\underline{c}_{L,i}$ is the acoustical impedance, resulting from the product of the density ρ_i, and the complex longitudinal wave velocity $\underline{c}_{L,i} = c_{L,i}.(1+j\delta_{cL})$, with losses $\delta_{cL} = c_L.\alpha_L/(2\pi f)$ resulting from the attenuation measurement α_L [12-13]. Thus, the transfer function $\underline{T}(f)$ between the first and second round-trip echoes in medium indexed 2 inserted between media indexed 1 and 3 leads to:

$$\underline{T}(f) = \frac{\underline{S}_{2r}(f)}{\underline{S}_{1r}(f)} = e^{+j2\pi f\frac{2d_2}{c_L}}.e^{-2d_2.\alpha_L}.\underline{R}_{21}.\underline{R}_{23}. \quad (3)$$

where $\underline{S}_{1r}(f)$ and $\underline{S}_{2r}(f)$ are spectra resulting from the first and second round-trip echoes in medium indexed 2, $\underline{R}_{21}$ and $\underline{R}_{23}$ (eq. (2)) are the reflection coefficients related to PMMA for indexes 1 and 3 and silicone oil for index 2. More precisely, the acoustical properties of constitutive materials are first evaluated from time-of-flight and amplitude ratio on pulse-echo measurements (Table 1):

Table 1: Acoustical properties of materials constituting the experimental device.

Materials	PMMA	Silicone oil
d (mm)	50	4
ρ (kg/m^3)	1175	965
c_L (m/s)	2740	980
c_T (m/s)	1365	–
δ_{cL} (%)	0.50	0.16

ρ:density; c_L, c_T: longitudinal and transverse wave velocities; δ_{cL}: losses.

The longitudinal wave velocity $c_L(f)$ and longitudinal wave attenuation $\alpha_L(f)$ are confirmed in agreement with those deduced from the transfer function $\underline{T}(f)$:

$$c_L(f) = 2\pi f \frac{2d_2}{Arg\left(\underline{T}(f)\right)}, \quad (4)$$

and

$$\alpha_L(f) = -\frac{1}{2d_2}\ln\left(\left|\frac{\underline{T}(f)}{\underline{R}_{21}.\underline{R}_{23}}\right|\right). \quad (5)$$

Therefore, it is possible to perform an accurate characterization measurement of the dispersion of the longitudinal wave velocity $c_L(f)$ (eq. (4)) and longitudinal wave attenuation $\alpha_L(f)$ (eq. (5)). This method allowed a precise characterization of the silicone oil layer [14-15].

2.2 Detectability

In order to extract reflectors dimensions from pulse-echo signals, their echoes must be clearly separated. This condition implies that the mold (here PMMA blocks) is to be thick enough not to disturb echoes from the fiber fabrics and air bubbles. The multiple echoes arrival dates from the first PMMA block are evaluated numerically. For instance, t_{LT} stands for the echo arrival date with a longitudinal (L) path and a transverse (T) path. Thus, the delays related to the first PMMA block gives a time exploration window between $t_{LL} = 2d_1/c_{L1} = 36.5$ µs and $t_{LT} = d_1.(1/c_{T1} + 1/c_{L1}) = 54.9$ µs due the LT conversion mode in the PMMA. The resulting time exploration window is $t_{ew} = t_{LT} - t_{LL} = d_1.(1/c_{T1} - 1/c_{L1}) = 18.4$ µs. The associated exploration depth is $z_2 = c_{oil}.t_{ew}/2 = 9$ mm in silicon oil, which is greater than the silicone oil gap fixed at 4 mm thick (Table 1).

In fact, this time exploration window t_{ew} is reduced by τ, this additional delay τ being the time of damping of the transducer echo. An estimation of this time of damping can be expressed as a function of the transducer's central frequency $f_0 = 10$ MHz and bandwidth $\Delta f_6 = 8$ MHz. The transducer's pseudo period is defined as $T_0 = 1/f_0 = 0.1$ µs. Particularly, for an echo with a gaussian envelope, its normalized duration t_n/T_0 for a given threshold at $-n$ dB can be related directly to the transducer's relative bandwidth $\Delta f_6/f_0$ [15]. This assumption of gaussian envelope (eq. (6)) is giving a good estimation of the transducer impulse response characteristics.

$$\frac{t_n}{T_0} \approx \frac{0,36\sqrt{n}}{(\Delta f_6 / f_0)}. \quad (6)$$

In our case, to the transducer's relative bandwidth was estimated around $\Delta f_6/f_0 = 80\%$. Thus, the theoretical detection limit at −6 dB, results in $t_6/T_0 = 1.1$ and the axial resolution $\Delta z_6 = c_{oil}.t_6/2 = 0.55.\lambda_0 = 55$ µm. As expected, the resolution is in the order of magnitude of the wavelength λ_0. Nevertheless, in order to separate two successive echoes, the condition must be extended with a higher threshold level at −40 dB. It leads to $t_{40}/T_0 = 2.8$ consider that a delay $\tau = 5.T_0$ is sufficient as minimum propagation time between two interfaces.

As a consequence, the round-trip delay of interest in pulse-echo mode t_{rt} is reduced and ranges from the end of the LL echo from the first PMMA block $t_{LL}+\tau$ up to the beginning of the t_{LT} echo, i.e. the time exploration window is modified with $t_{ew,\tau} = t_{LT} - (t_{LL}+\tau) = 37$ µs.

2.3 Signal processing

The raw data obtained from the phased array transducer is made of three dimensions: $s(x_{fl}, t_{rt}, t_{acq})$. The first dimension x_{fl} is spatial and corresponds to the focal law position, the second t_{rt} corresponds to the round-trip delay of reflection in pulse-echo mode (Figure 2) and the third t_{acq} is the acquisition date.

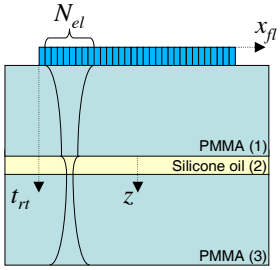

Figure 2: Phased array transducer: $N_{el} = 32$ active elements, at focal law position x_{fl} and acquisition date t_{acq}.

The assembly of the elementary A-scans obtained at each focal law results in a B-scan $s(x_{fl}, t_{rt})$ (Figure 3).

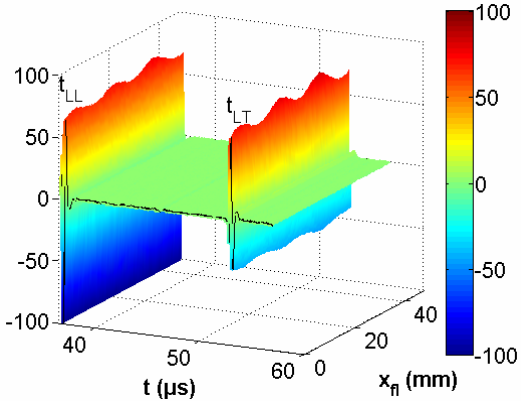

Figure 3: A-scan (solid black curve) and B-scan (colorscale map) obtained for a given acquisition date.

This B-scan is updated for each acquisition, resulting in $s(x_{fl}, t_{rt}, t_{acq})$. Moreover, the round-trip echo from a reflector at t_{rt} results in an equivalent depth in the silicone oil layer $z = c_{oil}.(t_{rt}-(t_{LL}+\tau))/2$ (Figure 2). The static component of the raw signal $s(x_{fl}, z, t_{acq})$ corresponds to the fibers (Figure 4 (a)). It is extracted from the raw data with an average on the acquisitions before bubble rising, i.e. up to $N_{acq,static}$:

$$s(x_{fl}, z, t_{acq}) = s_{static}(x_{fl}, z) + s_{dynamic}(x_{fl}, z, t_{acq}), \quad (7)$$

$$\text{with } s_{static}(x_{fl}, z) = \frac{1}{N_{acq,static}} \sum_{k=1}^{N_{acq,static}} s(x_{fl}, z, (k-1).dt_{acq}). \quad (8)$$

3 Results

The constitutive materials can be observed due to their echogenicity relatively to the main propagation medium, i.e. silicone oil. Therefore, the reflectors dimensions must be greater than the wavelength and their acoustical contrast must be significant. The first detection condition is related to the wavelength in silicone oil (paragraph 2.2) which was evaluated at λ_0 = 100 µm, what implies a theoretical axial resolution Δz_6 = 55 µm. Given that the reflectors are fibers ($d < \Delta z_6$) and fiber fabrics ($d > \Delta z_6$), only fiber fabrics can be observed acoustically. The second detection condition involves the reflection coefficient between materials indexed 1 and 2, i.e. $|R_{12}|^2 \approx |\underline{R}_{12}|^2$ (eq. (2), with $\delta_{cL} << 1$) and is estimated from these acoustical properties (Table 2):

Table 2: Immersed media properties.

Material	Z (kRa)	c_L (m/s)	ρ (kg/m^3)	d (mm)
Silicone oil (*s.o.*)	946	980	965	4
Glass fibers (*g.f.*)	12600	5640	2240	~0.1
Air (*air*)	0.440	340	1.3	~1

It results in high reflection values, since $|R_{s.o./g.f.}|^2 \approx 74\%$ between silicone oil and glass fibers, and $|R_{s.o./air}|^2 \approx 100\%$ between silicone oil and air. Therefore, the immersed fiber fabrics can be observed due to their echogenicity. As described in eq. (7) and (8), the echo signals are composed of a static component s_{static} and a dynamic one $s_{dynamic}$. These signals are processed to deliver images of the envelope of the B-scans $s = s_{dynamic}(x_{fl}, 1 < z < 4 \text{ mm}, t_{acq})$. This envelope processing (eq. (9)) results in high level signals for echogenic areas.

$$s_{env} = \left| s + j.Hilbert(s) \right| . \quad (9)$$

3.1 B-scan processing

The raw data $s(x_{fl}, z, t_{acq})$ can be seen as a sequence of B-scan maps $s(x_{fl}, z)$ associated to an acquisition date t_{acq}. A movie can illustrate the evolution of the B-scan as a function of time. Nevertheless, in our case, nothing but a nearly static image can be observed in this way: the so-called $s_{static}(x_{fl}, z)$. This is explained by the fact that the dynamic component is small compared to the static one. A subtraction of the static component to the raw data must be performed to highlight the signal corresponding to the moving air bubble (eq. (7) and (8)). As it is illustrated by Figure 4 (a), the three fabrics are detected at a depth 1.7 mm < z < 3.3 mm. The bubble is sliding along the glass fiber fabrics immersed in silicone oil, up to the top due to the Archimedes force [10-11]. The bubble is observed (Figure 4 (b)) at z = 2.2 mm depth at the acquisition date t_{acq} = 0.5 s, for which the bubble is localized at the position x_{fl} = 18 mm. Thus, the air bubble can be localized along two dimensions (x_{fl}, z) as a function of the acquisition date t_{acq}.

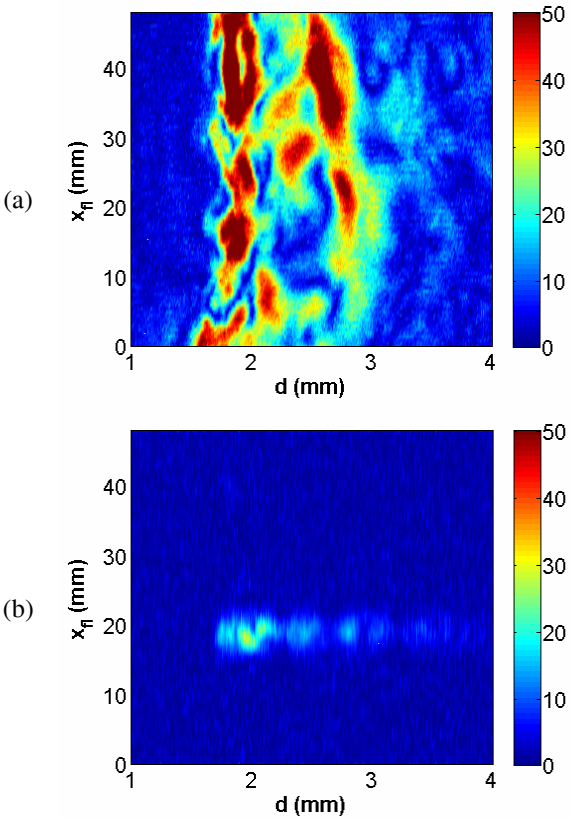

Figure 4: B-scans envelopes of a fibrous matrix including a moving air bubble: (a) meshes with $s_{static}(x_{fl}, z)$ and (b) bubble with $s_{dynamic}(x_{fl}, z, t_{acq} = 0.5 \text{ s})$.

3.2 C-scan processing

As illustrated by Figure 4 (b), both the position (x_{fl}, d) and velocity v_b of the bubble can be determined for each acquisition date t_{acq}. Here, the C-scan (Figure 5) was obtained by processing as follows:

$$s_C(t_{acq}, x_{fl}) = \max\left(s_{dynamic}(x_{fl}, z, t_{acq}) \right)_{\backslash 1 < z < 4 \text{ mm}} . \quad (10)$$

The bubble position x_{fl} is detected as a function of the acquisition date t_{acq}. As a result, the width and slope of the echogenic area are informing both on the bubble effective diameter D and displacement velocity v_b. In addition, the acoustic speckle is visible around the useful signal.

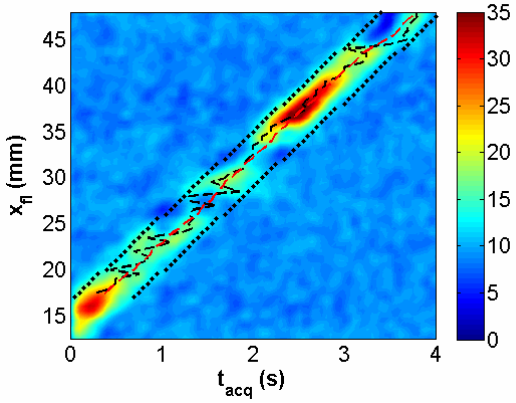

Figure 5: Detection of an air bubble in a fibrous matrix using a C-scan $s_C(t_{acq}, x_{fl})$ of the dynamic component $s_{dynamic}(t_{acq}, x_{fl})$, with 1 < z < 4 mm.

3.3 Bubble characteristics

More precisely, our interest is to identify the bubble position x_{fl} , its effective diameter D and velocity v_b from the processed C-scan s_C (Figure 5). An estimation of the instantaneous velocity $v_b = \Delta x_{fl}/\Delta t_{acq,c}$ of the bubble (Figure 6 (a)) can be extracted from the centroid value of the time $t_{acq,c}$ (eq. (11)) around a given focal law position x_{fl}.

$$t_{acq,c}(x_{fl}) = \frac{\sum_{k_{acq}=k_{acq,begin}}^{k_{acq,end}} s_C(k_{acq}, x_{fl}).t_{acq}(k_{acq})}{\sum_{k_{acq}=k_{acq,begin}}^{k_{acq,end}} s_C(k_{acq}, x_{fl})}. \quad (11)$$

These instantaneous measurements of the velocity v_b (Figure 6, dotted lines) are filtered (Figure 6, solid lines) due to signal perturbations from the fiber fabrics.

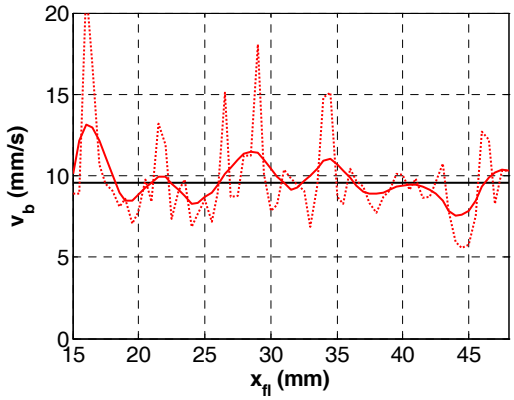

Figure 6: Estimation of the instantaneous measurements (dotted lines) and 3 points filtering (solid lines) of the velocity v_b of the bubble between fiber fabrics.

In addition, the effective diameter D of the air bubble can be estimated through the widths of the bubble along the focal law positions x_{fl} (Figure 6 (b)) or along the acquisition dates t_{acq} (Figure 6 (c)). More precisely, the form factor FF_{xfl} (eq. (12)) is evaluated along the t_{acq} axis, whereas the form factor FF_{tacq} (eq. (13)) is evaluated along the x_{fl} axis. This parameter is deduced from the width of the spot of the C-scan of the dynamic component s_C (eq. (10)):

$$FF_{x_{fl}} = \left(\Delta x_{fl}\right)_{x_{fl} \setminus \left(s_C > \frac{\max(s_C)}{2}\right)}. \quad (12)$$

$$FF_{t_{acq}} = v_{b,mean}.\left(\Delta t_{acq}\right)_{t_{acq} \setminus \left(s_C > \frac{\max(s_C)}{2}\right)}. \quad (13)$$

These form factors give similar results and their values mainly differ due to the estimation of the velocity. Indeed, the velocity mean value $v_{b,mean} \approx 9.6$ mm/s is taken into account. This result is in agreement with previous experiments in the same configuration. The effective diameter of the bubble D varies as a function of the bubble position between the fiber fabrics. As a result, the mean form factors can be estimated around $FF_{xfl,mean} \approx 4.7$ mm and $FF_{tacq,mean} \approx 4.3$ mm, with ~ ± 2 mm variations.

Therefore, the effective diameter of the air bubble along the x_{fl} axis is estimated around $D \approx 4.5$ mm, i.e. the bubble is flattened between the first and second fiber fabrics. In the same experimental setup, in the same viscous silicone oil, without fibers nor fiber fabrics, the velocity of a free perfectly spherical bubble with a diameter $D \approx 4.5$ mm should be theoretically around $v_{b,theory} \approx 45$ mm/s [10].

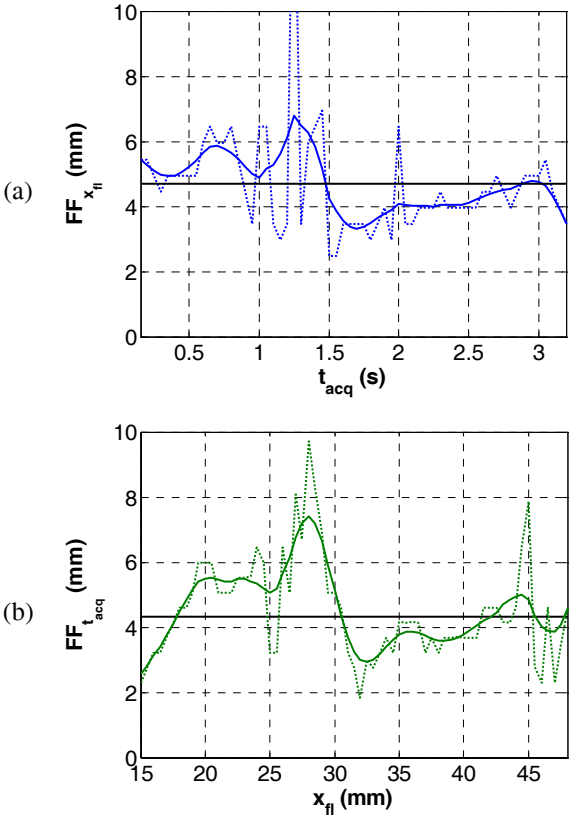

Figure 7: Estimations of the bubble effective diameter D with the instantaneous measurements (dotted lines) and 5 points filtering (solid lines) of the form factors (a) FF_{xfl} along t_{acq} and (b) FF_{tacq} along x_{fl}.

4 Conclusion

In this work, the feasibility of the detection of an air bubble displacement between fiber fabrics was performed. An experimental setup was fabricated to demonstrate this possibility, and to quantify the precision of the measurements of the velocity and effective diameter of an air bubble between fiber fabrics. Some basic signal processing were proposed and validated on the raw data obtained from the experimental setup. The perspectives of this work will consist in other configurations (phased array transducer, viscous fluid, fiber materials and fabrics, ...) and additional experimental results.

Acknowledgments

This work is supported by the CNRS and Région Haute-Normandie. The authors would like to thank their colleagues A. Ben Abdel Wahed, Y. Wielhorsky, L. Bizet and J. Bréard for their support.

References

[1] Ohnabe H., Masaki S., Onozuka M., Miyahara K., Sasa T., "Potential application of ceramic matrix composites to aero-engine components", *Composites: Part A* 30, pp.489-496, (1999).

[2] Saouab A., Bréard J., Lory P., Gardarein B., Bouquet G., "Injection simulations of thick composite parts manufactured by the RTM process", *Composites Science and Technology* 61, pp.445-451, (2001).

[3] Bréard J., Saouab A., Bouquet G., "Numerical simulation of void formation in LCM", *Composites: Part A* 34, pp.517-523, (2003).

[4] Le Riche R., Saouab A., Bréard J., "Coupled compression RTM and composite layup optimization", *Composites Science and Technology* 63, pp.2277-2287, (2003).

[5] Park C.H., Saouab A., Bréard J., Han W.S., Vautrin A., Lee W.I., "An integrated optimisation for the weight, the structural performance and the cost of composite structures", *Composites Science and Technology* 69, pp.1101-1107, (2009).

[6] Potter K.D., "The early history of the resin transfer moulding process for aerospace applications", *Composites: Part A* 30, pp.619-621, (1999).

[7] Mouton S., Teissandier D., Sébastian P., Nadeau J.P., "Manufacturing requirements in design: The RTM process in aeronautics", *Composites: Part A* 41, pp.125-130, (2010).

[8] Park C.H., Lebel A., Saouab A., Bréard J., Lee W.I., "Modeling and simulation of voids and saturation in liquid composite molding processes", *Composites Part A* 41, pp.658-668, (2011).

[9] Jeong H, Hsu D., "Experimental analysis of porosity-induced ultrasonic attenuation and velocity change in carbon composites", *Ultrasonics* 3, pp.195-203, (1995).

[10] Samet N., Maréchal P., and Duflo H., "Ultrasound monitoring of bubble size and velocity in a fluid model using phased array transducer", *NDT&E* 44, pp.621-627, (2011).

[11] Samet N., Ben Abdelwahed A., Maréchal P., Bizet L., Bréard J. "Détection de bulles en mouvement dans une préforme fibreuse par méthode ultrasonore", *20ème Congrès Français de Mécanique*, Lyon, August 29-16 (2011).

[12] Razansky D., Einziger P., Adam D., "Effectiveness of acoustic power dissipation in lossy layers", *J. Acoust. Soc. Am.* 116 (1), pp.84–89, (2004).

[13] Lenoir O., Maréchal P., "Study of plane periodic multilayered viscoelastic media: Experiment and simulation", *IEEE Int. Ultrason. Symp.*, Roma, September 20-23, (2009).

[14] Kline R.A., "Measurement of attenuation and dispersion using an ultrasonic spectroscopy technique", *J. Acoust. Soc. Am.* 76 (2), pp.498-504, (1984).

[15] Samet N., Maréchal P., and Duflo H., "Ultrasonic characterization of a fluid layer using a broadband transducer", *Ultrasonics* 52, pp.427-434, (2012).